State-of-Charge and State-of-Health Lithium-Ion Batteries' Diagnosis According to Surface Temperature Variation

Asmae El Mejdoubi, *Student Member, IEEE*, Amrane Oukaour, Hicham Chaoui, *Senior Member, IEEE*, Hamid Gualous, *Member, IEEE*, Jalal Sabor, and Youssef Slamani

***Abstract*—This paper presents a hybrid state-of-charge (SOC) and state-of-health (SOH) estimation technique for lithium-ion batteries according to surface temperature variation (STV). The hybrid approach uses an adaptive observer to estimate the SOH while an extended Kalman filter (EKF) is used to predict the SOC. Unlike other estimation methods, the closed-loop estimation strategy takes into account the STV and its stability is guaranteed by Lyapunov direct method. In order to validate the proposed method, experiments have been carried out under different operating temperature conditions and various discharge currents. Results highlight the effectiveness of the approach in estimating SOC and SOH for different aging conditions.**

***Index Terms*—Adaptive observer, extended Kalman filter (EKF), lithium-ion batteries, Lyapunov stability, parameters estimation, state-of-charge (SOC), state-of-health (SOH).**

I. Introduction

LITHIUM-ION batteries have received an increasing interest from the scientific community. Unlike other types of batteries such as lead acid, nickel cadmium (NiCd), and nickel metal hydride (NiMH), they offer higher energy efficiency and power density [1], [2]. Moreover, several other advantages such as low steady-state float current, light weight, small size, wide temperature operation range, rapid charge capability, long life cycle, low self-discharge rate, no memory effects, and the absence of hydrogen outgassing make them good candidates for many applications such as laptops, mobile phones, and electric vehicles [3]. However, optimal energy utilization and minimization of degradation effects are among the typical challenges to be faced.

Manuscript received February 1, 2015; revised April 13, 2015, June 11, 2015, August 11, 2015, and September 30, 2015; accepted November 15, 2015. Date of publication December 17, 2015; date of current version March 8, 2016.

A. El Mejdoubi is with the LUSAC Laboratory, Université de Caen Normandie, 14032 Caen, France, and also with ENSAM, Université Moulay Ismail, Meknes 50000, Morocco (e-mail: asmae.elmejdoubi@unicaen.fr)

A. Oukaour, H. Gualous, and Y. Slamani are with the LUSAC Laboratory, Université de Caen Normandie, 14032 Caen, France (e-mail: amrane.oukaour@unicaen.fr; youssef.slamani@unicaen.fr; hamid.gualous@unicaen.fr).

H. Chaoui is with the Center for Manufacturing Research, Department of Electrical and Computer Engineering, Tennessee Technological University, Cookeville, TN 38505 USA (e-mail: hchaoui@tntech.edu)

J. Sabor is with ENSAM, Université Moulay Ismail, Meknes 50000, Morocco (e-mail : sabor.jalal@hotmail.fr).

Color versions of one or more of the figures in this paper are available online at http://ieeexplore.ieee.org.

Digital Object Identifier 10.1109/TIE.2015.2509916

SOC and SOH are important aspects in battery management systems (BMSs) since they are considered, respectively, as the battery's energy and lifetime gauge. Therefore, bad SOC and SOH estimation ultimately result in damaging the battery and reducing its lifespan. Similar to other chemical-based energy storage systems, the battery's use generates irreversible physical and chemical changes, and hence its performance tends to deteriorate gradually over its lifetime. Several studies have been presented for lithium-ion battery calendar aging [4]–[7] and show an internal resistance increase and a capacity decrease. So, the definition of the end-of-life (EoL) of the battery depends on these aging indicators. The limit is generally set to 80% of the nominal capacity. In addition, Haifeng *et al.* [8] define another limit based on the internal resistance when it increases to 160% of its initial value for the same SOC and operating temperature condition. In calendar aging, the battery is stressed by many parameters such as the operating temperature and the depth-of-discharge [9]. Studies reveal that high operating temperature is more critical for a battery in calendar aging as opposed to low temperature. Grolleau *et al.* [4], [6] demonstrate that both high and low SOC have a significant effect on the battery's lifetime. On the other hand, Samba *et al.* [9] show experimentally that the surface temperature depends on the charge/discharge current, which influences the internal resistance of the battery.

Several classical SOC estimation techniques have been used for their simplicity [10]–[14]. A rational way to estimate a battery's SOC is by Coulomb counting method, also called amp-hour (Ah) balancing method [10], [11]. In this technique, battery's incoming and departing currents are integrated over time to determine SOC. But, this open-loop-based method results in a poor estimation precision since start-up and current sensor errors are also accumulated, which leads to a drift [12]. Moreover, the battery's capacity variations over its lifetime are not taken into account, which makes this method to have some serious drawbacks [10]. Nevertheless, it remains the simplest approach for real-time industrial applications. On the other hand, open-circuit voltage (OCV) can be used to determine a battery's SOC [13]–[16]. However, this technique requires the battery to be at equilibrium (i.e., no current flows through the battery for several minutes or hours). Some applications necessitate a continuous operation and do not allow batteries to reach an equilibrium state, which makes this method not suitable for online applications. Moreover, this relationship is affected by temperature and aging since capacity is known to gradually

decrease with charge and discharge cycles along with depth of discharge.

Various estimation methods have been reported in [17] for different battery's chemistries. Remarkably, lithium-ion stands as the most studied technology in this survey. Therefore, several robust and accurate estimation strategies are proposed at the cost of higher computational complexity [18], [19]. An accurate SOC estimation technique [20] is proposed using a reduced-order observer. However, it requires the knowledge of battery's parameters, which results in accuracy reduction as batteries age. This drawback has been overcome in [21], where an adaptive SOC estimation strategy is presented for lead–acid batteries. Considering an RC-equivalent circuit model, a real-time estimation of SOC of lithium polymer batteries is presented in [22] using an adaptive parameter identification based on RC parameters' update. A simple battery's model is used with a sliding mode observer to compensate for modeling uncertainties [23]. Taking temperature effects into account, charge/discharge characteristics under different constant currents are established experimentally for a NiMH battery [24]. Then, the SOC is derived from the experimental data. In [25], an optimization procedure uses measured current/voltage profiles to estimate online parameters of the battery's model. This way, the model is able to capture the relevant battery's dynamics and predicts the SOC based on voltage estimation. Referring to [17], many studies have been based on Kalman filter and its derivatives to estimate the SOC of lithium-ion batteries. Results show that Kalman filter provides satisfactory performance especially in tracking and stability. In [26], unscented Kalman filter (UKF) is used to estimate SOC using OCV–SOC operating temperature relationship. Orchard *et al.* [27] present a real-time SOC prognosis algorithm using particle filtering.

Neural networks and fuzzy logic have been credited in various applications such as powerful tools for systems subjected to different kinds of uncertainties [28], [29]. Numerous neural network models have been applied for the SOC and SOH estimation problems that have led a satisfactory performance [30], [31]. However, despite the success witnessed by neural networks, they remain incapable of incorporating any human-like expertise that was already acquired about the dynamics of the system in hand, which is considered as one of the main weaknesses of such soft computing methodologies. In [32], a fuzzy neural network (FNN) has been proposed to overcome this weakness. These techniques are among the intelligent management systems that can monitor the SOC and gradually reduce the load to prevent continuous operation at a low SOC. Thus far, a very few results have been reported taking the effect of temperature on the estimation of SOC and SOH into account.

The contribution of this paper is to propose a hybrid SOC and SOH estimation techniques for lithium-ion batteries taking temperature effects into account. The proposed estimation strategy combines adaptive and Kalman observers to estimate both SOC and SOH. The adaptive strategy consists of a Lyapunov-based adaptation law for online parameters' estimation. Therefore, the parameters are estimated since they, respectively, vary with SOC and SOH. Unlike other estimation methods, the proposed estimation algorithm achieves high accuracy and robustness, reduces the computation, and guaranties an important stability. In addition, the particularity of this algorithm compared to [33], is in the estimation of the internal resistance considering the variation of the surface temperature of the battery that influences its internal resistance value. Thus, the proposed method requires voltage, current, operating temperature, and surface temperature measurements. The effectiveness of the proposed method is verified by experiments for different aging states. The rest of this paper is organized as follows. The structure and study of lithium-ion battery calendar aging are presented in Section II. Section III outlines the circuit model for batteries. The proposed online diagnosis algorithm is detailed in Section IV. In Section V, experimental results are reported and analyzed. Finally, Section VI presents the conclusion with some remarks.

II. Battery Aging

A. Battery Calendar Aging

The reliability of batteries is estimated with different electrical tests that also give complementary information. They are of two test types: "dc voltage test" and "voltage cycling test."

Calendar life testing is often mentioned in [4]. The cells are prepared at different SOC values and stressed with different temperatures. The cell parameters as well as the internal resistance and the capacity are measured periodically with well-defined discharge conditions. In this study, a 20-Ah, 3.2 V lithium–iron–phosphate battery ($LiFePO_4$) is used in the experiments. For its characterization, the SOC cannot be constant. Consequently, the following protocol is applied.

1) Initially (before aging process), the battery is characterized at different constant currents and operating temperatures. The aim is the internal resistance (R) and the OCV–SOC characterization.
2) After that, the battery is placed inside a climatic chamber during a few days where its temperature is regulated at constant ambient temperature (60 °C) and the SOC of the battery is fixed at constant value (90%). This experiment is performed at a high temperature in order to accelerate the aging of the battery.
3) The battery is removed from the climatic chamber and is characterized at different currents and ambient temperatures as described previously. At the end of this stage, we put the battery again in the climatic chamber and we repeat the same measurements after a few days of aging.

B. Characterization Protocol

In order to validate the proposed estimation algorithm, a test bench has been designed, as presented in Fig. 1.

It is designed to perform three types of tests:

1) constant current, constant voltage (CCCV) charging method to charge the battery;
2) continuous discharging method using constant and variable currents profiles;
3) discontinuous discharging method to establish OCV–SOC characterization.

The two algorithms tests have been implemented under LabView and a USB-based data acquisition device

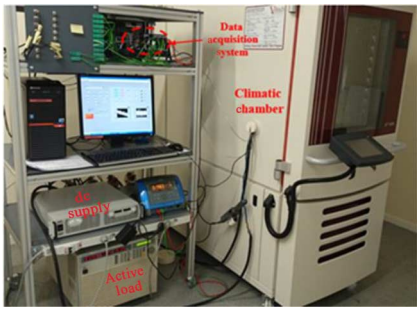

Fig. 1. Test bench.

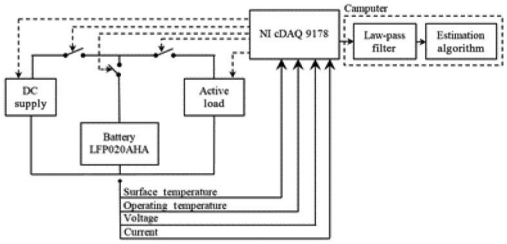

Fig. 2. Test bench design.

NI cDAQ-9178 has been used as a communication interface as shown in Fig. 2. The measurements are conducted with a sampling frequency of 10 Hz.

The characterization protocol was investigated under different conditions of operating temperature (10 °C, 22 °C, and 40 °C) and discharging current (constant currents of 6, 10, and 20 A, and variable current). For each couple of operating temperature and discharging current, the two experiments are carried out as follows. The battery has been charged using a constant current and when its voltage reaches the maximum voltage of 3.65 V, a constant voltage of 3.65 V is then applied until the battery's current reaches 0.01 A. As such, the battery is fully charged. Then, using continuous discharging, a discharge current is applied until the voltage reaches 2.8 V. For each discharge current, the necessary time to discharge the battery by 10% is calculated. Then, the battery is discharged each time by a 10% step. At each step, the battery is left idle for about 1 h to reach equilibrium and its OCV is measured.

Using the continuous discharging method described earlier, the battery's voltage V_b is measured for different SOC conditions. On the other hand, using the discontinuous discharging method, the OCV–SOC characterization is also established in various SOC conditions. Based on the two characterization techniques (i.e., OCV–SOC and V_b − SOC for 10% SOC step), the battery's internal resistance is calculated using the equation defined by Haifeng *et al.* [8]

$$R(\mathrm{SOC}_i) = \frac{\mathrm{OCV}(\mathrm{SOC}_i) - V_b(\mathrm{SOC}_i)}{I_b(\mathrm{SOC}_i)}. \quad (1)$$

Fig. 3 presents the characterization protocol that is used to validate the proposed estimation algorithm. It is important to note that this protocol is repeated for different aging phases:

1) using a constant current: 0 h (new cell), after 352, 544, and 650 h;
2) using a variable current: 0 h (new cell) and after 650 h.

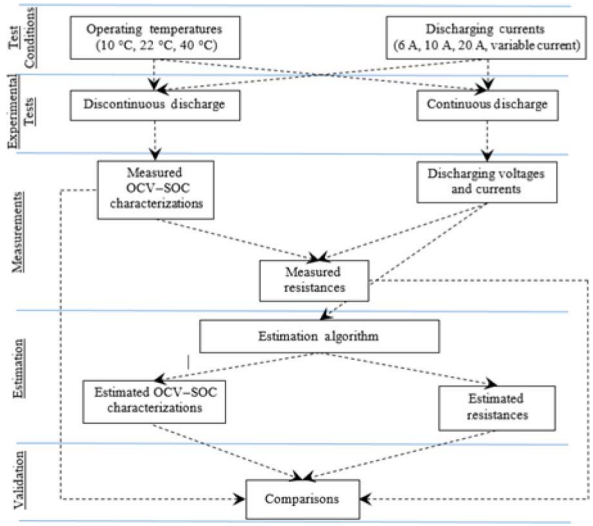

Fig. 3. Characterization protocol.

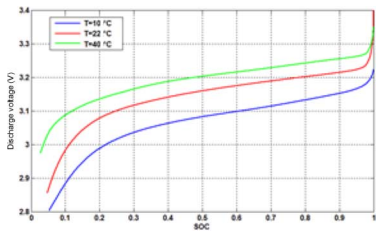

Fig. 4. Discharge voltage for different operating temperatures.

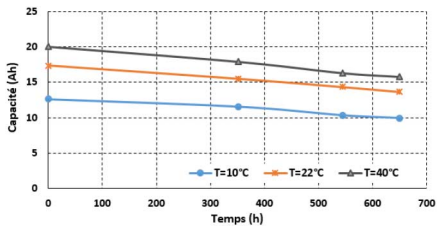

Fig. 5. Capacity evolution with aging time.

In order to examine the operating temperature effect, Fig. 4 presents the discharge voltage for the different operating temperatures using a constant current of 20 A. We notice that the discharge voltage is affected by the operating temperature. For high operating temperature, the discharge voltage is higher for the same SOC. It decreases as the temperature decreases [33]. This result is related to the decrease of both the lithium-ion diffusivity and the electrical conductivity of the electrolyte.

Experimental results for the battery capacity evolution versus aging time for full discharge after each phase of calendar aging are depicted in Fig. 5. As it is clearly shown in Fig. 5, the capacity of the battery decreases as the operating temperature decreases [34], [35].

In order to study the influence of the operating temperature on the OCV–SOC characterization, Fig. 6 presents the measured OCV–SOC characterizations for the three operating temperatures. We notice that the OCV decreases as the temperature decreases for the same SOC. The variation between the obtained results under 22 °C and the ones under 40 °C can

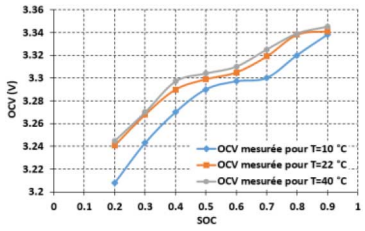

Fig. 6. Measured OCV–SOC characterizations for different temperatures.

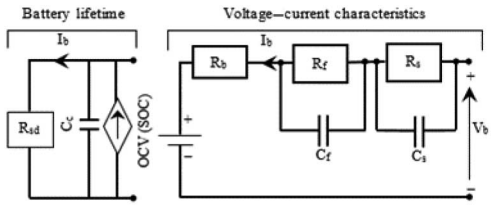

Fig. 7. Electric circuit of a lithium-ion battery.

be seen negligible. Unlike the variation between the obtained results under 22 °C and the ones under 10 °C, we notice that the difference is important, so we can conclude that the low temperature influence more the OCV–SOC characterization. These results are consistent with the ones obtained results in [16]. The OCV presents the base of the entropy coefficient that decreases as the operating temperature decreases [9]. We must add that the OCV variation is due to the hysteresis of the electromotive force, and the hysteresis is more pronounced at low SOC values [5], [9].

III. Lithium-Ion Model

A. Modeling

The lithium-ion batteries have a variety of applications. Based on those applications, the battery model can be classified into electrochemical, mathematical, intelligent, and electrical models. Nevertheless, the electrical model is the most used for estimation goals. In fact, several studies have been conducted for the electrical modeling of the lithium-ion battery, by using mathematical approaches presenting its four primary components: electrolyte, separator, anode, and cathode. Chen *et al.* [36] propose a particular model, as shown in Fig. 7.

This model is a combination of battery lifetime model on the left and voltage–current characteristics on the right. This RC network presents the terminal voltage dynamic response. The R_{sd} produces the self-discharge energy loss due to long time storage and C_c denotes the whole charge capacitor.

In order to simplify the model, and based on the results of Kim *et al.* [37], the voltage–current characteristics can be represented, as shown in Fig. 8. Slower transients arising from mass transport effects are assigned to the R_pC_p component, and the elements of that component are accordingly described as the diffusion resistance R_p and diffusion capacitance C_p [37].

The dynamic mathematical model is described by the following equations:

$$\dot{V}_p = \frac{1}{R_pC_p}V_p - \frac{1}{C_p}I_b \tag{2}$$

$$V_b = \text{OCV} + V_p + R_bI_b. \tag{3}$$

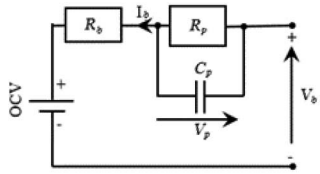

Fig. 8. Equivalent circuit model of voltage–current characteristic.

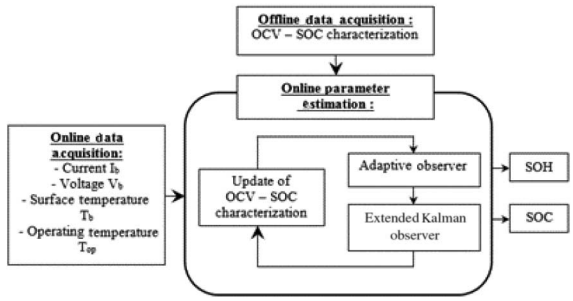

Fig. 9. Estimation algorithm.

where OCV is the open-circuit voltage, V_b is the battery voltage, I_b is the battery current, V_p is the voltage across R_pC_p network, and R_b is the resistance. The battery internal resistance is defined as the sum of the two resistances R_p and R_b.

B. Problem Statement

The aim of this study is to estimate the OCV, the internal resistance R_b, and the SOC since they are directly correlated to the battery's SOH. The system's measurable states are the battery voltage V_b, the current I_b, the battery surface temperature T_b, and the operating temperature T_{op}. In this work, the system's parameters are assumed to be *a priori* unknown. It is also assumed that these parameters along with the OCV are a slowly time-varying signals, so

$$\begin{cases} \dot{\text{OCV}} \approx 0 \\ \dot{R}_b \approx \dot{R}_p \approx 0 \\ \dot{C} \approx 0. \end{cases} \tag{4}$$

IV. Online Parameter Estimation

In order to estimate the online SOC and SOH, a closed-loop estimation scheme is proposed in Fig. 9.

As it is shown, the hybrid strategy combines two observers that are designed in the following section. The online estimation technique initially consists of OCV–SOC characterization using an extended Kalman observer. Then, the estimated OCV is fed to an adaptive observer to estimate the internal resistance. Therefore, the estimated battery's OCV and internal resistance are used since they, respectively, vary with SOC and SOH. The battery's EoL impedance REoL is taken as 160% brand new battery's impedance at the same condition of temperature, current, and SOC [8].

A. Extended Kalman Observer

Extended Kalman filter (EKF) has been successfully used for states' estimation [38], [39]. This method is well known

for its recursion that makes it suitable for real-time prediction. Although EKF has been used in various applications [38]–[40], this work is one of the scarce attempts of using EKF for lithium-ion parameters' estimation. In fact, Kalman filter tends to work well for linear systems. However, its performance deteriorates when applied to nonlinear systems. Since the system in hand is nonlinear, the proposed EKF implements a Kalman filter for a system dynamics that results from the linearization of the original nonlinear filter dynamics around the previous state estimates [38], [41].

Therefore, the EKF is used to estimate the state variables of a continuous nonlinear system that is linearized around its equilibrium point and is expressed by the following equation [38]:

$$\begin{cases} \dot{X}_2(t) = A.X_2(t) + B.u(t) + w(t) \\ Y(t) = E.X_2(t) + F.u(t) + v(t) \end{cases} \tag{5}$$

where $X_2(t)$ is the state vector for the extended Kalman observer, $Y(t)$ is the output, $w(t)$ is the state noise, $v(t)$ is the measurement noise, and t is the time index. It is assumed that noise is white, Gaussian, and known by covariance matrices w and v, respectively. In fact, this model must combine all deterministic system information. Based on (3), the system's variables are continuous.

In our algorithm, the main goal of this extended Kalman is to estimate the OCV–SOC characterization. It is important to note that the SOC is defined as a percentage of the total capacity and it is used to reflect the battery performance. The parameters to be estimated by the observer along with the input $u(t)$ and output $Y(t)$ are as follows:

$$\begin{cases} X_2 = [x_1\ x_2\ x_3]^T = [V_p\ \text{OCV}\ \text{SOC}]^T \\ u(t) = I_b(t) \\ Y(t) = V_b(t). \end{cases} \tag{6}$$

For SOC estimation, the most commonly used method is the Coulomb counting [16], defined as follows:

$$\text{SOC}(t) = \text{SOC}(t_0) + \int_{t_0}^{t} \frac{\eta.I_b}{Q_n} d\tau \tag{7}$$

where $\text{SOC}(t_0)$ is the initial value of the SOC, η is the Coulomb coefficient, and I_b is the battery current (positive for charge and negative for discharge).

Q_n is considered as the available capacity in the actual battery at a given aging condition. As such, Q_n is updated after each diagnosis process and taken to be equal to the real capacity provided by the battery at each charge/discharge measurement. This way, the capacity also decreases as the battery ages.

Based on (3), the assumption (4), and the SOC definition (7), the state vector derivation is given by

$$\dot{X}_2 = \begin{bmatrix} \dot{x}_1 \\ \dot{x}_2 \\ \dot{x}_3 \end{bmatrix} = \begin{bmatrix} \dot{V}_p \\ \dot{\text{OCV}} \\ \dot{\text{SOC}} \end{bmatrix} \tag{8}$$

$$\dot{X}_2 = \begin{bmatrix} \frac{1}{R_pC_p}.V_p - \frac{1}{C_p}I_b \\ 0 \\ \frac{\eta}{Q_n}.I_b \end{bmatrix} = \begin{bmatrix} \frac{1}{R_pC_p}.x_1 - \frac{1}{C_p}.u \\ 0 \\ \frac{\eta}{Q_n}.u \end{bmatrix}. \tag{9}$$

So, the matrix verify

$$\begin{aligned} A &= \begin{bmatrix} 1/R_pC_p & 0 & 0 \\ 0 & 0 & 0 \\ 0 & 0 & 0 \end{bmatrix} \\ B &= \begin{bmatrix} \frac{-1}{C_p} & 0 & \frac{\eta}{Q_n} \end{bmatrix}^T \\ E &= \begin{bmatrix} 1 & 1 & 0 \end{bmatrix} \\ F &= [R_b]. \end{aligned} \tag{10}$$

B. Adaptive Observer

Considering the derivation of (3) and the assumption (4),

$$\dot{V}_b = R_b\dot{I}_b + \dot{V}_p. \tag{11}$$

Referring to (2) and (11),

$$\dot{V}_b = R_b\frac{dI_b}{dt} - \frac{R_p + R_b}{R_pC_p}I_b + \frac{1}{R_pC_p}(V_b - \text{OCV}). \tag{12}$$

The model can be presented by a regression model

$$\dot{V}_b = X_1^T\theta \tag{13}$$

where

$$\begin{cases} \theta = \begin{bmatrix} \theta_1 & \theta_2 & \theta_3 \end{bmatrix}^T = \begin{bmatrix} R_b & \frac{R_p+R_b}{R_pC_p} & \frac{1}{R_pC_p} \end{bmatrix}^T \\ X_1 = \begin{bmatrix} \frac{dI_b}{dt} & -I_b & V_b - \text{OCV} \end{bmatrix}^T. \end{cases} \tag{14}$$

The estimated regression and parameter vectors are defined as

$$\begin{cases} \widehat{\theta} = \begin{bmatrix} \widehat{R}_b & \widehat{\frac{R_p+R_b}{R_pC_p}} & \widehat{\frac{1}{R_pC_p}} \end{bmatrix}^T \\ \widehat{X}_1 = \begin{bmatrix} \frac{dI_b}{dt} & -I_b & \widehat{V}_b & - & \widehat{\text{OCV}} \end{bmatrix}^T \end{cases} \tag{15}$$

where $\widehat{\text{OCV}}$ is the estimated value of OCV obtained by the Kalman observer. Therefore, define the estimation error as

$$e = V_b - \widehat{V}_b. \tag{16}$$

The battery voltage estimation law is defined as follows:

$$\dot{\widehat{V}}_b = \widehat{X}_1^T\widehat{\theta} + \lambda e \tag{17}$$

where λ is a positive constant. In [42], the authors estimate that the cell temperature must be monitored and controlled at a predetermined temperature level by a BMS. But, Samba *et al.* [9] prove experimentally that the surface temperature T_b varies depending on the battery current. Also, the surface temperature variation (STV) is the result of the Joule losses in the battery due to the charge/discharge current that influences the battery internal resistance only [9], [43].

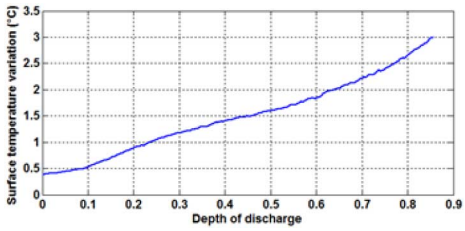

Fig. 10. STV with depth of discharge.

Samba *et al.* [9] also show that the side surface temperature of the battery is nearly uniform, except in the middle where the maximum temperature is measured. Therefore, this significant finding is taken into account by placing the surface temperature sensor in the middle of the battery side surface. Fig. 10 presents the STV of the battery discharged with a constant current profile of 20 A under an operating temperature of 40 °C.

It is important to note that the battery surface temperature increases when the depth of discharge increases. At the end of the discharge cycle, the STV reaches 3 °C.

So, we can deduce that

$$T_b = T_{\text{op}} + f(I_b) = T_{\text{op}} + \Delta T. \tag{18}$$

The internal resistance is defined as in [35]

$$R = R_p + R_b = \frac{\theta_2}{\theta_3}. \tag{19}$$

Then, we can write

$$\begin{aligned} R(T_b) &= R(T_{\text{op}} + \Delta T) \\ &= R_{p1}(T_{\text{op}}) + R_{p2}(\Delta T) + R_{b1}(T_{\text{op}}) + R_{b2}(\Delta T) \end{aligned} \tag{20}$$

where R_{p1} and R_{b1} are the components of the resistances R_p and R_b, respectively, resulted from the operating temperature; and R_{p2} and R_{b2} are the components of the resistances R_p and R_b, respectively, resulted from the STV.

Moreover, in [43], the authors prove experimentally that the operating temperature influences the battery voltage response for the same condition of current. So, referring to (3) and (20), we have

$$V_b(T_{\text{op}}) = \text{OCV}(T_{\text{op}}) + V_p(T_{\text{op}}) + R_{b1}(T_{\text{op}})\, I_b \tag{21}$$

where R_{b1} is the component of resistance R_b resulted from the operating temperature and presented directly in the electric model. So, in order to consider the STV in the resistance estimation, we consider a nonlinear system verifying Theorem 1.

Theorem 1: The estimation law in (17) guarantees the closed-loop estimation stability with the following adaptation law:

$$\dot{\widehat{\theta}} = \Gamma\left(\widehat{X}_1 + \Delta T \vartheta\right) e \tag{22}$$

where $\Gamma = \begin{bmatrix} \gamma_1 & \gamma_2 & \gamma_3 \end{bmatrix}^T$ and γ_i is a positive adaptation gain and $\vartheta = \begin{bmatrix} 1 & 1 & 1 \end{bmatrix}^T$.

Proof 1: Choose the following Lyapunov candidate:

$$V\left(e, \tilde{\theta}\right) = \frac{1}{2}e^2 + \frac{1}{2}\tilde{\theta}^T \Gamma^{-1} \tilde{\theta} \tag{23}$$

such that $\tilde{\theta} = \theta - \theta$.

Taking the derivative, the Lyapunov function leads to

$$\dot{V} = \dot{e}e + \dot{\tilde{\theta}}^T \Gamma^{-1} \tilde{\theta}. \tag{24}$$

Substituting for $\dot{e}$ yields

$$\dot{V} = \left(\dot{V}_b - \dot{\widehat{V}}_b\right) e - \dot{\widehat{\theta}}^T \Gamma^{-1} \tilde{\theta}. \tag{25}$$

It is important to note that $\dot{\tilde{\theta}} = -\dot{\widehat{\theta}}$, since parameters θ are considered to be slowly time varying such as $\dot{\theta} \simeq 0$. Substitute for $\dot{V}_b$ and $\dot{\widehat{V}}_b$

$$\dot{V} = (\xi - \lambda e)\, e - \dot{\widehat{\theta}}^T \Gamma^{-1} \tilde{\theta} \tag{26}$$

where $\xi = X_1^T \theta - \widehat{X}_1^T \widehat{\theta}$ is the approximation uncertainty. Add and subtract $\widehat{X}_1^T \theta$

$$\xi = \tilde{X}_1^T \theta + \widehat{X}_1^T \tilde{\theta} \tag{27}$$

where $\tilde{X}_1 = X_1 - \widehat{X_1}$. Therefore,

$$\dot{V} = \tilde{X}_1^T \theta e + \widehat{X}_1^T \tilde{\theta} e - \dot{\widehat{\theta}}^T \Gamma^{-1} \tilde{\theta} - \lambda e^2. \tag{28}$$

Setting the adaptation law as in (22) leads to

$$\dot{V} = \left(\tilde{X}_1^T \theta - \vartheta^T \tilde{\theta} \Delta T\right) e - \lambda e^2. \tag{29}$$

Applying Young's inequality [44],

$$\dot{V} \leq \frac{1}{2\alpha}\Psi^2 + \frac{\alpha}{2}e^2 - \lambda e^2 \tag{30}$$

where $\Psi = \widehat{X}_1^T \theta - \vartheta^T \tilde{\theta} \Delta T$. Setting $\lambda = \frac{\alpha}{2} + \beta$ yields

$$\dot{V} \leq \frac{1}{2\alpha}\Psi^2 - \beta e^2. \tag{31}$$

Choosing $\alpha > 0$ and $\beta > 0$, so that $\dot{V} \leq 0$ guarantees the system's stability to a neighborhood of $e = 0$. Therefore, the system is stable in the sense of Lyapunov. The neighborhood of $e = 0$ is a region defined by the approximation error $\tilde{\Psi}$ and get smaller as $\tilde{\Psi} \to 0$. ■

V. Experimental Results

A. Estimation Results Obtained Under Constant Current Profile

1) Estimate Internal Resistance Validation: Using the aforementioned experimental protocol results for a constant current, Fig. 11 illustrates the internal resistance evolution for the different currents and operating temperatures, and a comparison between the estimated internal resistance defined by (19) and calculated one in (1).

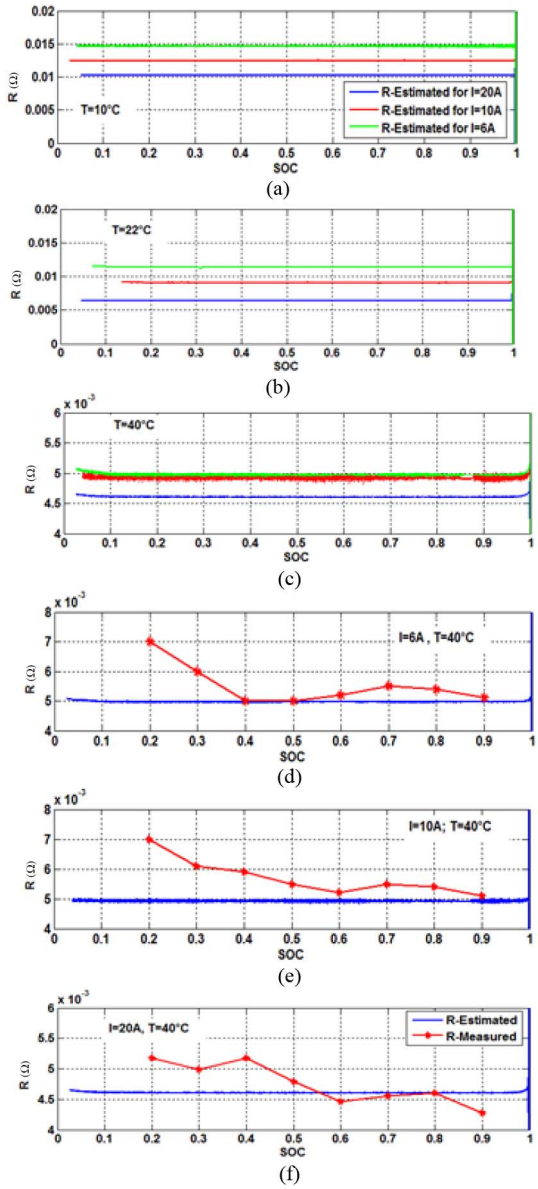

Fig. 11. Internal resistance evolutions for various operating temperatures and discharge currents. (a) $T = 10\ ^{\circ}\mathrm{C}$. (b) $T = 22\ ^{\circ}\mathrm{C}$. (c) $T = 40\ ^{\circ}\mathrm{C}$. (d) Estimated and measured resistance for operating temperature $T = 40\ ^{\circ}\mathrm{C}$ and discharge current $I = 6$ A. (e) Estimated and measured resistance for operating temperature $T = 40\ ^{\circ}\mathrm{C}$ and discharge current $I = 10$ A. (f) Estimated and measured resistance for operating temperature $T = 40\ ^{\circ}\mathrm{C}$ and discharge current $I = 20$ A.

Comparing the estimated and measured results for the SOC between 0.4 and 0.9, we notice that the relative error is low with a maximum value reaching 15.92%, as presented in Table I.

It is noteworthy from (1) that the estimation's accuracy is directly correlated to the measurement's quality of both the battery's voltage and current as well as the OCV. Therefore, any voltage or current measurement inaccuracy has a direct impact on the battery's internal resistance estimation's precision. Henceforth, low resistance values combined with low sensors' precision and measurements' noise make accurate estimation a difficult task to undertake in real life.

It should be mentioned that the electrolyte assures a link between the two electrodes: the cathode and the anode,

TABLE I
RELATIVE ERROR OF RESISTANCE ESTIMATION FOR OPERATING TEMPERATURE $T = 40\ ^{\circ}\mathrm{C}$ AND CONSTANT CURRENT

SOC	0.4	0.5	0.6	0.7	0.8	0.9
40°C–6A	0.48%	0.4%	4.34%	9.27%	7.79%	2.37%
40°C–10A	15.92%	9.81%	4.61%	9.82%	8.14%	2.74%
40°C–20A	11.19%	3.96%	3.13%	1.09%	0.21%	7.27%

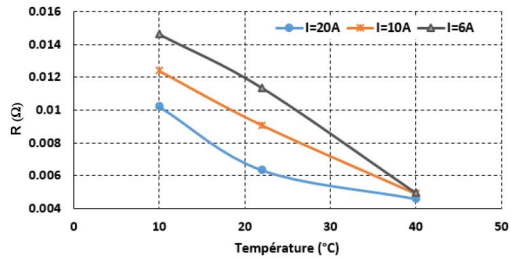

Fig. 12. Estimated internal resistance in various currents and operating temperatures.

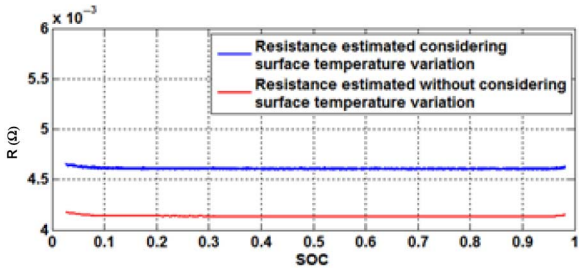

Fig. 13. Comparison between the estimated resistance considering the STV and without considering the STV.

presented in the electric model by the internal resistance of the battery. So, the resistance evolution is an image of the electrolyte parameters such as the viscosity and the reaction speed [9], [38]. We notice that for the same operating temperature, the resistance decreases as the discharge current increases. Based on the load transfer presented by Butler–Volmer equation, the speed of the redox reaction of the electrolyte is a function of the current. In high discharge current, the reaction speed is more important causing a decrease of the resistance. In addition, Fig. 12 shows that the resistance increases as the operating temperature decreases. This is due to the increase of the electrolyte's viscosity that generates the redox reaction speed decrease [9], [39].

In order to evaluate the impact of the STV, the resistance has been estimated using the same hybrid observer without considering the STV. In this case, the STV is considered to be equal to zero, i.e., $\Delta T = T_{\mathrm{op}} - T_b = 0$.

Fig. 13 presents a comparison between the resistance estimated by considering the STV and the resistance estimated without considering the STV for a battery discharged using a constant current profile of 20 A under an operating temperature of 40 °C.

The obtained results show that the resistance estimated without considering the STV is smaller than the resistance estimated considering the STV. The difference between the two

TABLE II
RELATIVE ERROR FOR RESISTANCE ESTIMATION CONSIDERING AND WITHOUT CONSIDERING THE STV

SOC	0.4	0.5	0.6	0.7	0.8	0.9
With STV	10.91%	1.8%	4.88%	1.42%	0.32%	3.08%
Without STV	20.19%	12.04%	6.04%	9.14%	10.13%	3.18%

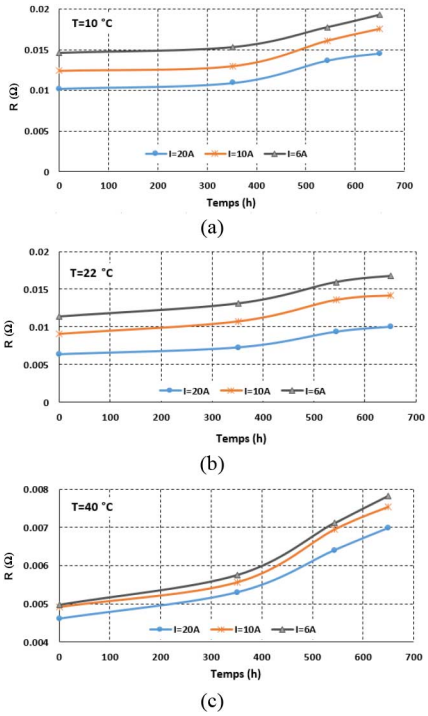

Fig. 14. Estimated internal resistance evolutions during lifetime for various operating temperatures. (a) $T = 10\,^{\circ}\mathrm{C}$. (b) $T = 22\,^{\circ}\mathrm{C}$. (c) $T = 40\,^{\circ}\mathrm{C}$.

resistances corresponds to the components of the resistance resulted from the STV as presented in (19).

Compared to the resistance measured in the same characterization conditions presented in Fig. 11(f), Table II presents a comparison between the relative error for the resistance estimated by considering the STV and without considering the STV.

In the case of estimation without considering the STV, the relative error, presented in Table II, achieves a maximum value of 20.19% compared to the maximum relative error of 10.91% in the case of estimation considering the STV.

2) Internal Resistance Evolution During the Battery Lifetime: As it is shown in Fig. 14, the resistance increases during the battery lifetime regardless of the operating temperature or the discharging current. Therefore, the internal resistance is considered as a crucial parameter to define the battery's SOH.

3) Estimate OCV–SOC Characterization Validation: Fig. 15 presents the OCV–SOC characterizations for different temperatures with comparison between the estimated and measured ones. Referring to the theoretical studies, the discharging current does not influence the OCV–SOC characterization. Therefore, whatever the discharging current

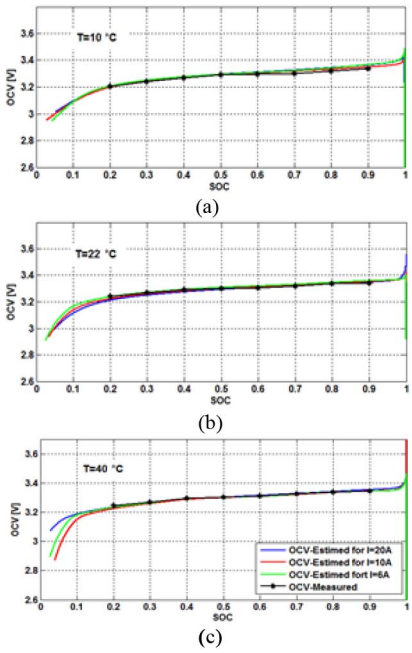

Fig. 15. OCV-SOC characterizations for new cell at various operating temperatures. (a) $T = 10\,^{\circ}\mathrm{C}$. (b) $T = 22\,^{\circ}\mathrm{C}$. (c) $T = 40\,^{\circ}\mathrm{C}$.

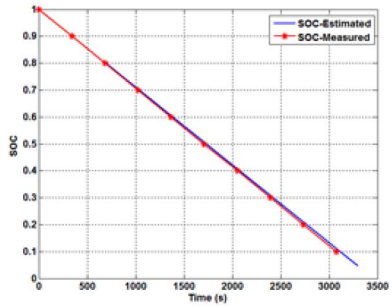

Fig. 16. Comparison between measured and estimated SOC.

applied, the OCV–SOC characterization is invariable for the same temperature condition.

So, the estimated results confirm this theoretical theory, we note that the difference between the OCV–SOC characterizations corresponding to each discharging current is negligible, for the different operating temperatures. In other part, and in order to validate the proposed estimation algorithm, for each operating temperature, the comparison between the estimated and the measured OCV–SOC characterizations shows an important convergence between the two characterizations for a SOC varying between 20% and 90%. The relative error obtained is less than 0.69%.

In order to validate the estimated SOC, Fig. 16 shows a comparison between the estimated SOC and the measured one using the Coulomb counting method. This result corresponds to the case of a new cell discharged using a constant current profile of 20 A under 22 °C. The SOC initial state is set to 80%.

Perfect tracking is achieved and the error remains very small, i.e., less than 0.62%, during all experiment. The high accuracy of the proposed observer is clearly shown in this experiment. We also note that the initial state does not influence the SOC estimation performance.

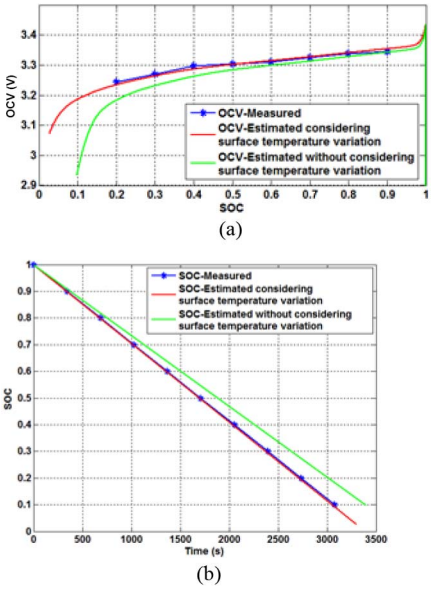

Fig. 17. Comparison between measured and estimated parameter considering and without considering STV. (a) OCV. (b) SOC.

TABLE III
RELATIVE ERROR FOR OCV AND SOC ESTIMATION CONSIDERING AND WITHOUT CONSIDERING THE STV

	OCV		SOC	
	With STV	Without STV	With STV	Without STV
0.2	0.3%	1.8%	0.93%	10.12%
0.3	0.21%	1.16%	0.91%	10.1%
0.4	0.3%	1.01%	0.90%	10.08%
0.5	0.06%	0.605%	0.88%	10.02%
0.6	0.12%	0.33%	0.88%	9.94%
0.7	0.09%	0.42%	0.88%	9.93%
0.8	0.06%	0.33%	0.88%	9.92%
0.9	0.27%	0.06%	0.88%	9.79%

The same objective that consists to evaluate the impact of the STV on the OCV and SOC estimation is discussed in this section.

Fig. 17 presents a comparison between the measured and estimated values with and without considering the STV for each parameter of the discharged battery using a constant current profile of 20 A under an operating temperature of 40 °C.

Compared to the measured values of OCV and SOC, Table III presents a comparison between the relative error for the parameter estimated considering the STV and without considering the STV.

The relative error for the SOC estimation has been calculated based on the measured and estimated time t_m and t_e, respectively, required to discharge a full battery to achieve SOC_i

$$\text{relative error}(\mathrm{SOC}_i) = \left| \frac{t_m\left(\mathrm{SOC}_i\right) - t_e(\mathrm{SOC}_i)}{t_m(\mathrm{SOC}_i)} \right|. \quad (32)$$

In the case of estimation without considering the STV, the relative error for OCV estimation achieves a maximum value of 1.8% compared to the maximum relative error of 0.3% in the case of estimation considering the STV. On the other hand, the maximum relative error of SOC estimation achieves 10.12% without STV and 0.93% with STV.

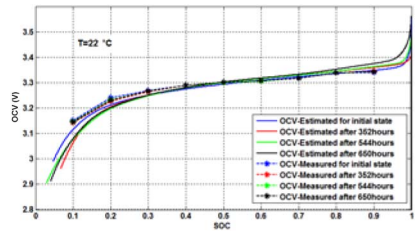

Fig. 18. OCV–SOC characterization evolution during lifetime.

4) OCV–SOC Characterization Evolution During the Battery Lifetime: In order to study the evolution of the OCV–SOC characterization during the battery lifetime, we have compared the OCV–SOC characterization for different aging states. Fig. 18 presents the different estimated and measured OCV–SOC characterizations. We notice that the variation is negligible from one aging state to another, not only for the measured but also for the estimated characterization. Referring to [16], there is no significant difference for the OCV–SOC characterization during the lifetime, which is consistent with the obtained results, with a maximum relative error of 1.58%.

In order evaluate the convergence properties of the proposed diagnosis model, Fig. 19 shows the relative error evolution between the measured and the estimated discharge voltage using the adaptive and extended Kalman observers. This result corresponds to the case of a constant discharge current of 6 A and a constant operating temperature of 10 °C. As it is observed, the initial relative errors of both observers decay gradually to zero. The asymptotic stability and convergence presented in *Proof 1* is clearly shown. It is noteworthy that the convergence speed of the adaptive observer can be improved by increasing its adaptation parameter rates at the expense of more noise at the estimate.

The proposed diagnosis method is a hybrid SOC and SOH estimation technique for lithium-ion batteries according to STV. The battery's STV is taken into account for internal resistance estimation.

Several estimation techniques, such as dc characterization, Coulomb counting method, and electrochemical impedance spectroscopy (EIS), have been proposed for lithium-ion batteries diagnosis. However, most of these techniques do not take into account the effect of surface temperature and they are not adapted for real time estimation. On the other hand, well-known benchmark techniques such as dc characterization and Coulomb counting method are used in this paper to validate the proposed approach. However, the calculated values with these techniques are also obtained without considering the STV, which makes accurate benchmark a difficult task to undertake.

B. Estimation Results Obtained Under Variable Current Profile

In this experiment, the ability of the proposed hybrid observer to cope with disturbance is evaluated. The chosen discharge current profile, depicted in Fig. 20, is usually used in vehicular application [45].

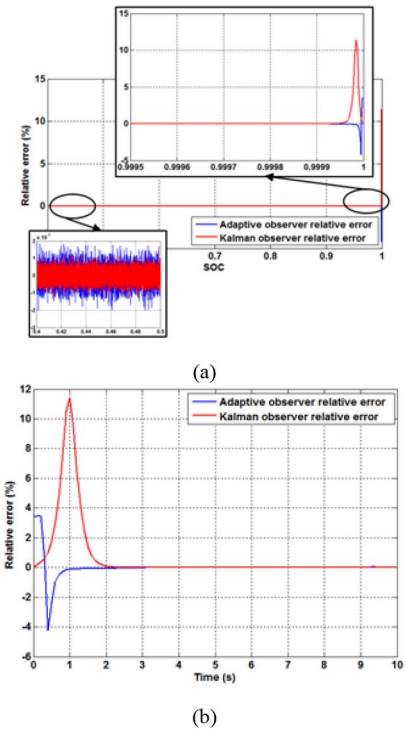

Fig. 19. Relative error evolution. (a) With SOC variation. (b) With time variation.

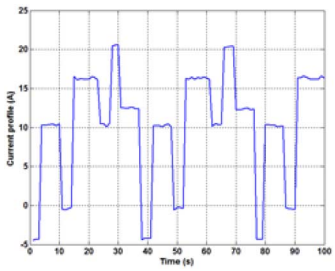

Fig. 20. Applied current profile.

A time-varying current profile is used to mimic the driving behavior of electric vehicles (including regenerative braking) and its effect on the battery's performance and SOH. The chosen current profile is based on the Federal Urban Driving Schedule, which is an automobile industry standard for urban driving used for a number of years for electric vehicle performance testing [43], [46], [47].

This current profile is used to characterize the battery for two aging phases: 0 h (new cell) and after 650 h. The current profile for this experiment shown in Fig. 20 is repeated for 7000 s to completely discharge a fully charge battery. The performance of the proposed observer in estimating the battery's parameters is revealed in Fig. 21.

Despite of the presence of discontinuity in the current profile, the estimation is similar to the constant current experiment's case. Therefore, the resistances and OCV–SOC characterization converge with no observable chattering or instability. The robustness of the proposed hybrid observer is checked and the obtained results are satisfactory.

On another aspect, comparison between EKF and its nonlinear counterpart such as, UKF has been performed for several applications [48], [49]. Results demonstrated a negligible gain

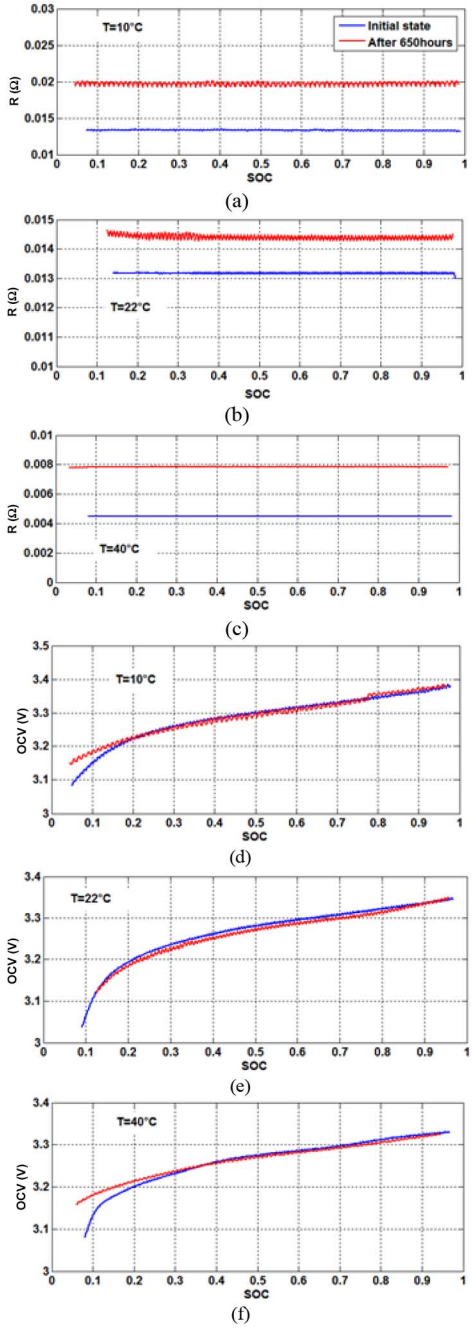

Fig. 21. Estimated results using a variable current. (a) Estimated resistances for $T = 10\ ^{\circ}\mathrm{C}$. (b) Estimated resistances for $T = 22\ ^{\circ}\mathrm{C}$. (c) Estimated resistances for $T = 40\ ^{\circ}\mathrm{C}$. (d) Estimated OCV-SOC characterization for $T = 10\ ^{\circ}\mathrm{C}$. (e) Estimated OCV–SOC characterization for $T = 22\ ^{\circ}\mathrm{C}$. (f) Estimated OCV-SOC characterization for $T = 40\ ^{\circ}\mathrm{C}$.

in performance compared to the added computational burden introduced by UKF. In [49], EKF and UKF yield the same accuracy. In online applications such as in electric vehicles where the onboard computation power is limited, EKF remains more suitable without compromising the system's performance.

This work assumes the availability of temperature sensors that are usually available in BMSs of hybrid and electric vehicles (HEVs) since thermal management of all cells is a major concern in the design of lithium-ion battery packs for HEVs. It is noteworthy that in the case of partially measured temperature, several techniques are available in the literature to estimate the temperature distribution for lithium-ion batteries [50], [51].

VI. Conclusion

In this paper, an online SOC and SOH estimation method was presented for lithium-ion batteries. The proposed strategy capitalizes on the capabilities of Kalman filtering for the design of an extended Kalman observer to estimate SOC. The battery's STV is taken into account for internal resistance estimation. Moreover, the adaptive estimation technique achieves online robust SOH estimation. The proposed online diagnosis model achieves SOC and SOH estimation in real time and does not require the interruption of the system's operation as opposed to the dc characterization and EIS methods. The effectiveness of the proposed online observer is shown through a set of experiments in discharging mode. Due to battery's inherent hysteresis, the experimental validation of the proposed method in charging mode is to be considered as a future work to confirm its effectiveness for both operating modes. Results highlight its good performance in parameters' estimation for different conditions of operating temperature, discharging current, and battery's aging conditions.

References

[1] M.-Y. Kim, C.-H. Kim, J.-H. Kim, and G.-W. Moon, "A chain structure of switched capacitor for improved cell balancing speed of lithium-ion batteries," *IEEE Trans. Ind. Electron.*, vol. 61, no. 8, pp. 3989–3999, Aug. 2014.

[2] A. Kuperman, U. Levy, J. Goren, A. Zafransky, and A. Savernin, "Battery charger for electric vehicle traction battery switch station," *IEEE Trans. Ind. Electron.*, vol. 60, no. 12, pp. 5391–5399, Dec. 2013.

[3] A. Ranjbar, A. Banaei, A. Khoobroo, and B. Fahimi, "Online estimation of state of charge in li-ion batteries using impulse response concept," *IEEE Trans. Smart Grid*, vol. 3, no. 1, pp. 360–367, Mar. 2012.

[4] S. Grolleau *et al.*, "Calendar aging of commercial graphite/LiFePO4 cell–Predicting capacity fade under time dependent storage conditions," *J. Power Sources*, vol. 255, pp. 450–458, 2014.

[5] V. Pop, H. J. Bergveld, P. P. L. Regtien, J. H. G. Op het Veld, D. Danilov, and P. H. L. Notten, "Battery aging and its influence in the electromotive force," *J. Electrochem. Soc.*, vol. 154, pp. A744–A740, 2007.

[6] S. Grolleau, A. Delaille, and H. Gualous, "Predicting lithium-ion battery degradation for efficient design and management," in *Proc. Elect. Veh. Symp. Exhib. (EVS'27)*, Barcelona, Spain, Nov. 2013, pp. 1–6.

[7] J. Schmalstieg, S. Kabitz, M. Ecker, and D. U. Sauer, "From accelerated aging tests to a lifetime prediction model: Analyzing lithium-ion batteries", in *Proc. Elect. Veh. Symp. Exhib. (EVS'27)*, Barcelona, Spain, Nov. 2013, pp. 1–12.

[8] D. Haifeng, W. Xuezhe, and S. Zechang, "A new SOH prediction concept for the power lithium-ion battery used on HEVs," in *Proc. Veh. Power Propul. Conf. (VPPC'09)*, Dearborn, MI, USA, Sep. 7–10, 2009.

[9] A. Samba *et al.*, "Development of an advanced two-dimensional thermal model for large size lithium-ion pouch cells," *Electrochim. Acta*, vol. 117, pp. 246–254, 2014.

[10] T. Hansen and C.-J. Wang, "Support vector based battery state of charge estimator," *J. Power Sources*, vol. 141, no. 2, pp. 351–358, Mar. 2005.

[11] S. Duryea, S. Islam, and W. Lawrance, "A battery management system for stand-alone photovoltaic energy systems," *IEEE Ind. Appl. Mag.*, vol. 7, no. 3, pp. 67–72, Jun. 2001.

[12] L. Liu, L. Wang, Z. Chen, C. Wang, F. Lin, and H. Wang, "Integrated system Identification and state-of-charge estimation of battery systems," *IEEE Trans. Energy Convers.*, vol. 28, no. 1, pp. 12–23, Mar. 2013.

[13] M. Gholizadeh and F. Salmasi, "Estimation of state of charge, unknown nonlinearities, and state of health of a lithium-ion battery based on a comprehensive unobservable model," *IEEE Trans. Ind. Electron.*, vol. 61, no. 3, pp. 1335–1344, Mar. 2014.

[14] M. Shahriari and M. Farrokhi, "Online state-of-health estimation of VRLA batteries using state of charge," *IEEE Trans. Ind. Electron.*, vol. 60, no. 1, pp. 191–202, Jan. 2013.

[15] M. Doyle, T. P. Fuller, and J. Newman, "Modeling of galvanostatic charge and discharge of the lithium/polymer/insertion cell," *J. Electrochem. Soc.*, vol. 140, no. 6, pp. 1526–1533, 1993.

[16] B. Pattipati, B. Balasingam, G. V. Avvari, K. R. Pattipati, and Y. Bar-Shalom, "Open circuit voltage characterization of lithium-ion batteries," *J. Power Sources*, vol. 269, pp. 317–333, Jul. 2014.

[17] M. Ugras Cuma and T. Koroglu, "A comprehensive review on estimation strategies used in hybrid and battery electric vehicles," *Renew. Sustain. Energy Rev.*, vol. 42, pp. 517–531, 2015.

[18] Z. Chen, Y. Fu, and C. Mi, "State of charge estimation of lithium-ion batteries in electric drive vehicles using extended kalman filtering," *IEEE Trans. Veh. Technol.*, vol. 62, no. 3, pp. 1020–1030, Mar. 2013.

[19] H. He, R. Xiong, X. Zhang, F. Sun, and J. Fan, "State-of-charge estimation of the lithium-ion battery using an adaptive extended kalman filter based on an improved thevenin model," *IEEE Trans. Veh. Technol.*, vol. 60, no. 4, pp. 1461–1469, May 2011.

[20] H. Chaoui and P. Sicard, "Accurate state of charge (SOC) estimation for batteries using a reduced-order observer," in *Proc. IEEE Int. Conf. Ind. Technol. Southeastern Symp. Syst. Theory*, Auburn, AL, 2011, pp. 39–43.

[21] H. Chaoui, P. Sicard, and H. Ndjana, "Adaptive state of charge (SOC) estimation for batteries with parametric uncertainties," in *Proc. IEEE/ASME Adv. Intell. Mechatron. Int. Conf.*, Montreal, ON, Jul. 2010, pp. 703–707.

[22] H. Rahimi-Eichi, F. Baronti, and M.-Y. Chow, "Online adaptive parameter identification and state-of-charge coestimation for lithium-polymer battery cells," *IEEE Trans. Ind. Electron.*, vol. 61, no. 4, pp. 2053–2061, Apr. 2014.

[23] I.-S. Kim, "Nonlinear state of charge estimator for hybrid electric vehicle battery," *IEEE Trans. Power Electron.*, vol. 23, no. 4, pp. 2027–2034, Jul. 2008.

[24] A. Szumanowski and Y. Chang, "Battery management system based on battery nonlinear dynamics modeling," *IEEE Trans. Veh. Technol.*, vol. 57, no. 3, pp. 1425–1432, May 2008.

[25] P. Van Bree, A. Veltman, W. Hendrix, and P. van den Bosch, "Prediction of battery behavior subject to high-rate partial state of charge," *IEEE Trans. Veh. Technol.*, vol. 58, no. 2, pp. 588–595, Feb. 2009.

[26] Y. Xing, W. He, M. Pecht, and K. L. Tsui, "State of charge estimation of lithium-ion batteries using the open-circuit voltage at various ambient temperatures," *Appl. Energy*, vol. 113, pp. 106–115, 2014.

[27] M. E. Orchard, P. Hevia-Koch, B. Zhang, and L. Tang, "Risk measures for particle-filtering-based state-of-charge prognosis in lithium-ion batteries," *IEEE Trans. Ind. Electron.*, vol. 60, no. 11, pp. 5260–5269, Nov. 2013.

[28] H. Chaoui and P. Sicard, "Adaptive fuzzy logic control of permanent magnet synchronous machines with nonlinear friction," *IEEE Trans. Ind. Electron.*, vol. 59, no. 2, pp. 1123–1133, Feb. 2012.

[29] H. Chaoui, P. Sicard, J. Lee, and A. Ng, "Neural network modeling of cold-gas thrusters for a spacecraft formation flying test-bed," in *Proc. IEEE Conf. Ind. Electron. Soc.*, Montreal, QC, 2012, pp. 2619–2621.

[30] M. Charkhgard and M. Farrokhi, "State-of-charge estimation for lithium-ion batteries using neural networks and EKF," *IEEE Trans. Ind. Electron.*, vol. 57, no. 12, pp. 4178–4187, Dec. 2010.

[31] H.-T. Lin, T.-J. Liang, and S.-M. Chen, "Estimation of battery state of health using probabilistic neural network," *IEEE Trans. Ind. Informat.*, vol. 9, no. 2, pp. 679–685, May 2013.

[32] F.-J. Lin, M.-S. Huang, P.-Y. Yeh, H.-C. Tsai, and C.-H. Kuan, "DSP-based probabilistic fuzzy neural network control for li-ion battery charger," *IEEE Trans. Power Electron.*, vol. 27, no. 8, pp. 3782–3794, Aug. 2012.

[33] H. Chaoui, N. Golbon, I. Hmouz, R. Souissi, and S. Tahar, "Lyapunov-based adaptive state of charge and state of health estimation for lithium-ion batteries," *IEEE Trans. Ind. Electron.*, vol. 62, no. 3, pp. 1610–1618, Mar. 2015.

[34] N. Yang, X. Zhang, and G. Li, "State-of-charge estimation for lithium ion batteries via the simulation of lithium distribution in the electrode particles," *J. Power Sources*, vol. 272, pp. 68–78, 2014.

[35] C-S. Kim, K. M. Jeong, K. Kim, and C.-W. Yi, "Effect of capacity ratio between anode and cathode on electrochemical properties for lithium polymer batteries," *J. Electrochimica Acta*, vol. 155, pp. 431–436, Feb. 2015.

[36] M. Chen and G. A. Rincon-Mora, "Accurate electrical battery model capable of predicting runtime and I-V performance," *IEEE Trans. Energy Convers.*, vol. 21, no. 2, pp. 504–511, Jun. 2006.

[37] J. Kim, J. Shin, C. Chun, and B. Cho, "Stable configuration of a Li-Ion series battery pack based on a screening process for improved voltage/SOC balancing," *IEEE Trans. Power Electron*, vol. 27, no. 1, pp. 411–424, Jan. 2012.

[38] R. Toscano and P. Lyonnet, "A kalman optimization approach for solving some industrial electronics problems," *IEEE Trans. Ind. Electron.*, vol. 59, no. 11, pp. 4456-4464, Nov. 2012.

[39] D. Andre, A. Nuhic, T. Soczka-Guth, and D.U. Sauer, "Comparative study of a structured neural network and an extended Kalman filter for state of health determination of lithium-ion batteries in hybrid electric vehicles," *Eng. Appl. Artif. Intell.*, vol. 26, pp. 951–961, 2012.
[40] K. Szabat and T. Orlowska-Kowalska, "Performance improvement of industrial drives with mechanical elasticity using nonlinear adaptive kalman filter," *IEEE Trans. Ind. Electron.*, vol. 55, no. 3, pp. 1075–1084, Mar. 2008.
[41] R. Xiong, H. He, F. Sun, and K. Zhao, "Evaluation on state of charge estimation of batteries with adaptive extended kalman filter by experiment approach," *IEEE Trans. Veh. Technol.*, vol. 62, no. 1, pp. 108–117, Jan. 2013.
[42] W. Waag, S. Käbitz, and D.-U. Sauer, "Experimental investigation of the lithium-ion battery impedance characteristic at various conditions and aging states and its influence on the application," *Appl. Energy*, vol. 102, pp. 885–897, 2013.
[43] N. Omar *et al.*, "Lithium iron phosphate based battery – Assessment of the aging parameters and development of cycle life model," *Appl. Energy*, vol. 113, pp. 1575–1585, 2014.
[44] R. A. Freeman and P. V. Kokotovic, "Lyapunov design," in *The Control Handbook*, vol. 77. Boca Raton, FL, USA: CRC, 1996, pp. 932–940.
[45] M. El Baghdadi *et al.*, "Vehicle power flow simulations based on trajectories with inductive charging systems," in *Proc. Eur. Conf. Power Electron. Appl. (EPE'13)*, Lille, France, Sep. 3–5, 2013, pp. 1–10.
[46] K. Young, C. Wang, L. Y. Wang, and K. Strunz, "Electric vehicle battery technologies," in *Electric Vehicle Integration into Modern Power Networks, Power Electronics and Power Systems*, R. Garcia-Valle and J. A. Peças Lopes. New York, NY, USA: Springer, 2013.
[47] F. Marra, G. Y. Yang, C. Træholt, E. Larsen, C. N. Rasmussen, and S. You, "Demand profile study of battery electric vehicle under different charging options," in *Proc. IEEE Power Energy Soc. Gen. Meeting*, San Diego, CA, USA, Jul. 22–26, 2012, pp. 1–7.
[48] M. St.-Pierre and D. Gingras, "Comparison between the unscented Kalman filter and the extended Kalman filter for the position estimation module of an integrated navigation information system," in *Proc. IEEE Intell. Veh. Symp.*, Jun. 14–17, 2004, pp. 831–835.
[49] J. J. LaViola, "A comparison of unscented and extended Kalman filtering for estimating quaternion motion," in *Proc. Amer. Control Conf.*, Denver, CO, USA, Jun. 2003, pp. 2435–2440.
[50] Y. Xiao, D. Torregrossa, and M. Paolone, "Surface temperature estimation of li-ion battery via thermal impulse response technique," in *Proc. IEEE Appl. Power Electron. Conf. Expo. (APEC'15)*, Charlotte, NC, USA, Mar. 2015, pp. 1089–1095.
[51] Y. Kim, S. Mohan, J. B. Siegel, A. G. Stefanopoulou, and Y. Ding, "The estimation of temperature distribution in cylindrical battery cells under unknown cooling conditions," *IEEE Trans. Control Syst. Technol.*, vol. 22, no. 6, pp. 2277–2286, Nov. 2014.

Asmae El Mejdoubi (S'15) was born in Morocco in 1988. She received the Engineering degree in electromechanical engineering from the Ecole Nationale Supérieure d'Arts & Métiers "ENSAM," Meknès, Morocco, in 2012. Currently, she is working toward a joint Ph.D. degree in electrical engineering between the Université de Caen Normandie, Caen, France, and l'ENSAM de l'Université Moulay Ismail, Meknes, Morocco.

Her research interests include the area of energy storage, more specifically, supercapacitors and lithium-ion batteries, state-of-health and state-of-charge diagnosis, and aging estimation.

Amrane Oukaour was born in Algeria in 1963. He received the Ph.D. degree in electrical engineering from the Pierre and Marie Curie University (Paris IV), Paris, France in 1993.

From 1995 to 2003, he was an Associate Professor with the Antilles and French Guyana University. Since 2003, he has been an Associate Professor with the Caen Normandie University, Caen, France. His research interests include the field of diagnosis of the aging states of power sources (batteries, supercapacitors, and fuel cells).

Hicham Chaoui (S'01–M'12–SM'13) received the B.Sc. degree in electrical engineering from the Institut Supérieur du Génie Appliqué (IGA), Casablanca, Morocco, in 1999, and the M.A.Sc. degree in electrical engineering, the M.Sc. degree in computer science (with honors), the Graduate degree in project management, and the Ph.D. degree in electrical engineering (with honors) from the Université du Québec à Trois-Rivières, Trois-Rivières, QC, Canada, in 2002, 2004, 2007, and 2011, respectively.

His career has spanned both academia and industry in the field of intelligent control and renewable energies. Prior to his academic career, he held various engineering and management positions including Vice-President Innovation and Technology Development at TDE Techno Design in Montreal, QC, Canada. Currently, he is an Assistant Professor with Tennessee Technological University, Cookeville, TN, USA, and an Adjunct Professor with the Université du Québec à Trois-Rivières, Montréal, QC, Canada. He has coauthored more than 50 journal and conference publications. He serves regularly as a Reviewer for many prestigious scientific journals. His research interests include adaptive and nonlinear control theory, intelligent control, robotics, mechatronics, electric motor drives, and energy storage and management.

Dr. Chaoui was a recipient of the Best Thesis Award for doctoral dissertation (health, natural science, and engineering) and the Governor General of Canada Gold Medal Award.

Hamid Gualous (M'14) was born in Morocco in 1967. He received the Ph.D. degree in electronics from the University Paris XI Orsay, Orsay, France, in 1994.

From 1996 to 2009, he was an Associate Professor with the FEMTO-ST Laboratory, University of Franche-Comte, Besançon, France. Currently, he is a Full Professor with the Université de Caen Normandie, Caen, France, and the Director of the LUSAC Laboratory. His research interests include energy storage devices, marine renewable energies, and energy management systems for smart grids.

Jalal Sabor received the Ph.D. degree in engineering science from the Institut National des Sciences Appliquées (INSA), Rouen, France, in 1995.

Currently, he is a Professor of Industrial Computer Science with the Ecole Nationale Supérieure d'Arts & Métiers (ENSAM), Université Moulay Ismail, Meknes, Morocco. He is also a member of the LSMI Laboratory. He is also the Head of the research team control steering and supervision systems. His research interests include intelligent management of energy, smart grid, control and supervision systems, and architecture based on multi-agent systems and fuzzy logic.

Youssef Slamani received the Ph.D. degree in control systems from the University of Caen Normandie, Caen, France, in 1988.

Currently, he is an Associate Professor in control systems and signal processing with the IUT of Cherbourg (University of Caen Normandie) and a member of the LUSAC Laboratory. His research interests include the fields of systems and control theory.